Design of a Dual-Band Microstrip Loop Antenna With Frequency-Insensitive Reactance Variations for an Extremely Small Array

Maeng Chang Kang, Hosung Choo, *Senior Member, IEEE*, and Gangil Byun, *Member, IEEE*

***Abstract*— This paper proposes a design for a dual-band microstrip loop antenna with an electromagnetically coupled feed for frequency-insensitive reactance variations. The antenna consists of two microstrip loops that are coupled to each other, and the ratio of the electric and magnetic coupling strengths is adjusted to lower the reactance slope. To demonstrate the suitability of the proposed feeding mechanism, antenna characteristics are measured in a full-anechoic chamber, and its operating principle is interpreted from a circuit standpoint. The results prove that the proposed structure exhibits a frequency-insensitive behavior without a significant gain reduction in the presence of strong mutual coupling.**

***Index Terms*— Controlled reception pattern antenna, frequency-insensitive antenna, microstrip loop antenna.**

I. Introduction

MICROSTRIP patch antennas have been widely adopted as individual elements of controlled reception pattern antenna arrays due to their directive patterns toward the upper hemisphere and the ease of achieving dual-band properties. In addition, their low-profile characteristics allow for reducing the antenna size by employing high-dielectric substrates, which are essential in recent wireless communications systems to overcome size restrictions [1]. Further size reduction can be achieved by employing additional structures, such as slot insertion [2]–[5], fractal patterns [6]–[9], and shorting pins [10]–[12]. However, impedance matching and radiation properties become sensitive to frequency variations because of narrow matching bandwidths. This frequency-sensitive behavior of the antenna with reduced aperture sizes often degrades the radiation properties, especially in an extremely small array, as the frequency response of antenna characteristics is easily shifted by the strong mutual coupling effect. Although a capacitively coupled feed has been proposed to relieve this frequency-sensitive behavior, it requires an additional layer to place an extra feeding patch [13]–[15] or rectangular unit cells [16]–[18]. Therefore, there has been an increasing demand for array antennas with reduced frequency sensitivity to be applied in electrically restricted aperture areas [19]–[21].

In this paper, we propose a frequency-insensitive microstrip loop antenna with an electromagnetically coupled feed as individual elements of extremely small arrays with restricted aperture areas. The proposed antenna helps to prevent significant gain reduction caused by the mutual coupling effect between array elements and consists of upper and lower microstrip loops printed on high-dielectric ceramic substrates. The lower loop is directly connected to the external chip coupler (XC1400P-03S from Anaren) [22] for quadrature phase excitation, and the upper loop is then coupled to the lower loop through electromagnetic (EM) fields. The ratio of the electric and magnetic coupling strengths is adjusted by varying the width and the vertical placement of the loops. The frequency-insensitive characteristic can be achieved by this proposed feeding mechanism accompanied by the loop resonators, since it lowers the reactance slope and minimizes the gain variations between the two resonant frequency bands. To demonstrate the feasibility of the proposed feeding structure, the frequency sensitivity of reactance (FSR) is defined to use as a figure of merit to evaluate the sensitiveness, and radiation characteristics of a fabricated antenna are measured in a full-anechoic chamber. We also examine the near-EM fields around the antenna and build an equivalent circuit model to analyze the operating principle of the proposed feeding mechanism. The results show that the proposed structure is suitable for achieving frequency-insensitive reactance variations without a significant gain reduction in an extremely small array.

II. Design Approach and Proposed Antenna

Fig. 1 shows the proposed dual-band antenna with an electromagnetically coupled feed structure. The antenna consists of upper and lower microstrip loops that are printed on a high-dielectric ceramic substrate ($\varepsilon_r = 20$, $\tan\delta = 0.035$), and the strip widths of the two loops are determined by w_c and w_2. The edge lengths of the loops are adjusted by parameters l_1 and l_2, so that the total loop lengths become approximately one effective wavelength in the GPS L_1 and L_2 bands. The lower loop is located in the substrate at a height of h_1 and is directly connected to two ports of the hybrid chip coupler. The central angle of the two feeding positions is fixed

Manuscript received November 3, 2016; revised March 7, 2017; accepted April 7, 2017. Date of publication April 28, 2017; date of current version May 31, 2017. This research was supported in part by the Civil Military Technology Cooperation and in part by the Basic Science Research Program through the National Research Foundation of Korea (NRF), funded by the Ministry of Education under Grant NRF-2014R1A1A2055813. *(Corresponding author: Gangil Byun.)*

M. C. Kang is with the RF/Microwave Team, LIG Nex1 Co. Ltd., Yongin 16911, South Korea.

H. Choo is with the School of Electronic and Electrical Engineering, Hongik University, Seoul 121-791, South Korea.

G. Byun is with the Research Institute of Science and Technology, Hongik University, Seoul 121-791, South Korea (e-mail: kylebyun@gmail.com).

Digital Object Identifier 10.1109/TAP.2017.2694862

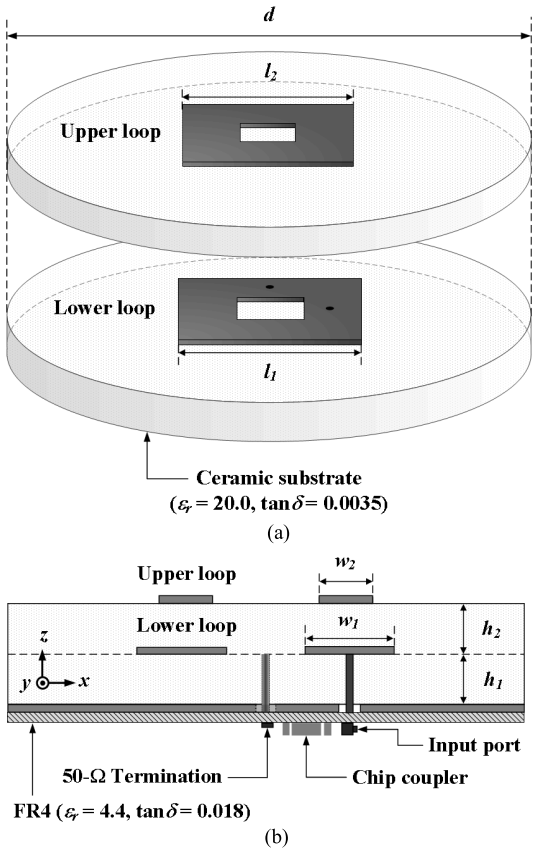

Fig. 1. Geometry of the proposed antenna. (a) Top view. (b) Side view.

at 90°, and the distance from the antenna center to each port is determined by parameter l_f. By applying this design scheme, the antenna periodically achieves the vertical and horizontal polarizations, which circulates the electric currents on the microstrip loops. Note that the reason for adopting the loop radiators is that the ratio of the electric and magnetic coupling strengths can be adjusted by varying the width and the vertical placement of the loops. For example, a strong electric coupling can be achieved when w_1 and w_2 are constrained to greater than 3 mm, and the strength of the magnetic coupling can be increased when the value of h_2 is maintained to be smaller than that of h_1. Table I lists the detailed values for the design parameters that are optimized using the genetic algorithm [23]. As expected, the total loop lengths, determined by l_1 and l_2, are approximately one effective wavelength at each resonant frequency. In addition, the two loops have wide strip widths of 5.5 and 6.7 mm, respectively, to maximize the electric coupling strength and are placed in close proximity at an interval of $h_2 = 4$ mm ($< h_1$) to create tighter magnetic coupling.

Fig. 2 shows the photographs of the fabricated antenna. A ceramic powder from Samboo Ceramics, Co. Ltd. was pasted and sintered to make a high-dielectric ceramic substrate, and the loops were printed on the substrate using the copper deposition mechanism. We also fabricated a printed circuit board to integrate the hybrid chip coupler, coplanar wave guides, and a 50-Ω termination chip for quadrature phase excitation. Then, the radiation characteristics of the fabricated

TABLE I
OPTIMIZED VALUES OF THE PROPOSED ANTENNA

Parameter	Value
d	127 mm
h_1	8 mm
h_2	4 mm
l_1	19.2 mm
l_2	18.4 mm
l_f	6.3 mm
w_1	5.5 mm
w_2	6.7 mm

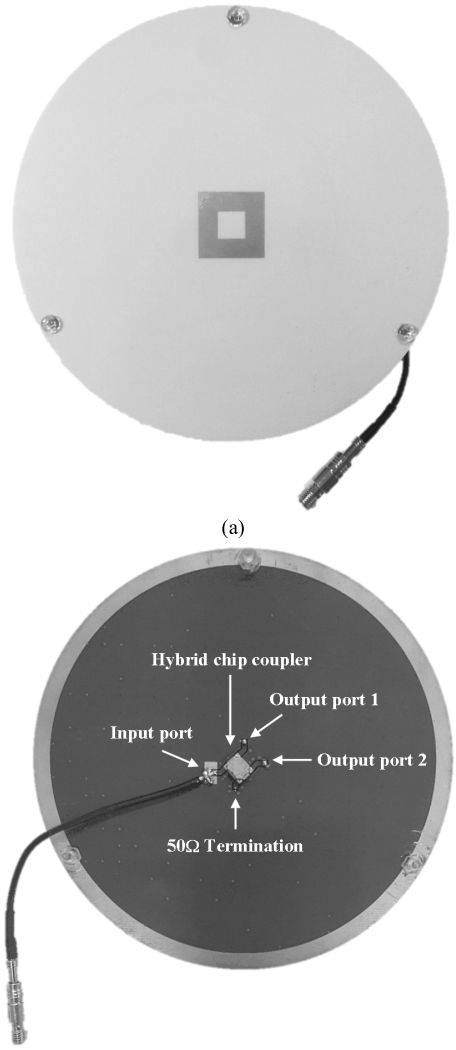

Fig. 2. Photographs of the fabricated antenna. (a) Top view. (b) Bottom view.

antenna were measured in a full-anechoic chamber to demonstrate the suitability of the proposed feeding mechanism, which will be discussed in the following section.

III. MEASUREMENT

Fig. 3 shows a comparison of the measured and simulated reflection coefficients. To compute the simulated values,

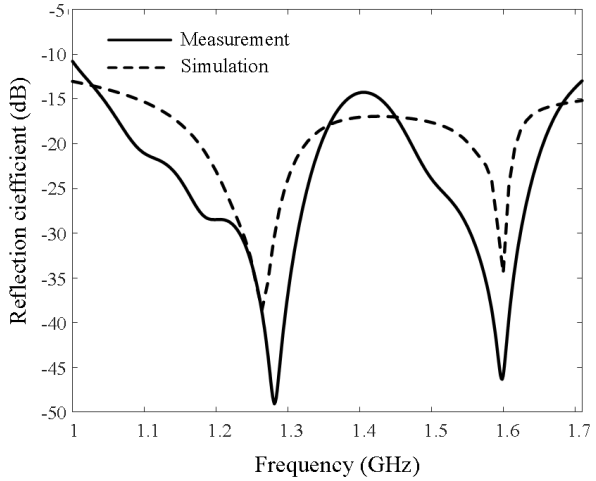

Fig. 3. Reflection coefficients of the proposed antenna.

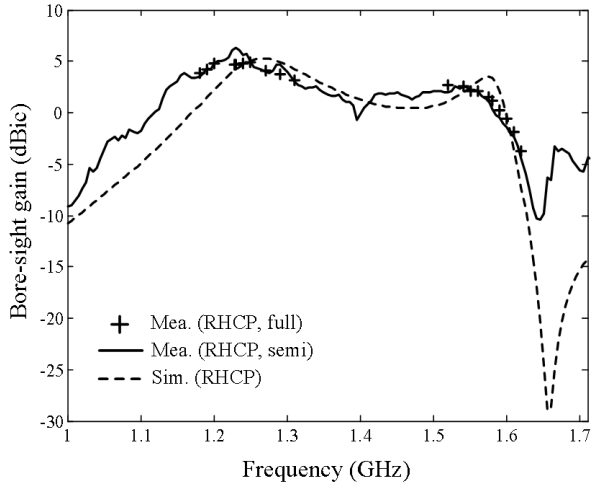

Fig. 4. Bore-sight gain of the proposed antenna.

the coupler circuit with four ports (two outputs, one input, and one isolation) was modeled using Advanced Design Software [24], and two output ports of the chip coupler were connected to a two-port scattering matrix obtained from the proposed antenna. Thus, the input reflection coefficients (Γ_{in}) of the antenna connected to the feeding network can be calculated as

$$\Gamma_{\text{in}} = \frac{1}{2}\{(-S_{11} + S_{22}) + j(S_{12} + S_{21})\} \tag{1}$$

where S_{11}, S_{12}, S_{21}, and S_{22} are the components of the two-port scattering matrix calculated as a function of frequency using the FEKO EM simulation software [25]. The dashed line indicates the simulated reflection coefficients of Γ_{in}, which have values of -29.5 and -26.9 dB at 1.575 and 1.227 GHz, respectively. The measured results are -35 dB (1.575 GHz) and -29.4 dB (1.227 GHz), and they show a good agreement with the simulated data.

Fig. 4 shows the measured bore-sight gains compared to the simulated data. The dashed line indicates the simulated results, and the measured values obtained from the full-anechoic chamber are marked by "+" symbols. We also present the experimental results, conducted in a semianechoic chamber,

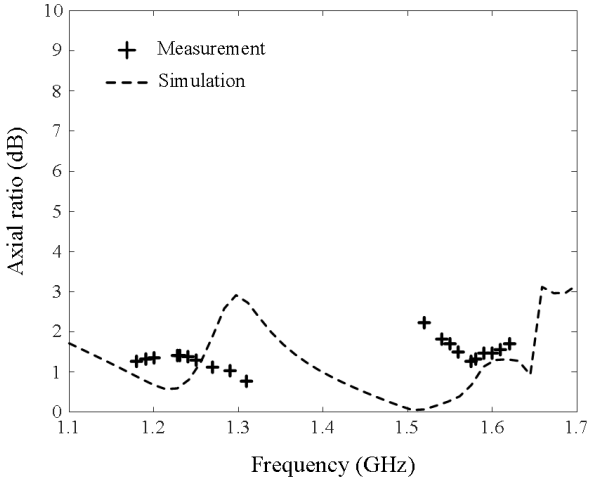

Fig. 5. AR of the proposed antenna.

as a solid line, to provide a continuous curve according to the frequency. The measured values are 1.5 dBic at 1.575 GHz and 4.7 dBic at 1.227 GHz, and the gain is greater than 0 dBic between the two resonant frequency bands, from 1.17 to 1.6 GHz (430 MHz) due to the frequency-insensitive behavior of the proposed feeding mechanism.

Fig. 5 provides a comparison between the measured and simulated axial ratios (ARs). To calculate the measured ARs, the orientation of a linearly polarized standard horn antenna is rotated for vertical and horizontal polarizations, and the received field magnitudes are considered to calculate the ratio of the major and minor axes in the polarization ellipse [26]. The antenna is circularly polarized with measured AR values of 1.3 and 1.4 dB at 1.575 and 1.227 GHz, respectively, and the simulated values are 0.5 dB (1.575 GHz) and 0.8 dB (1.227 GHz). The antenna maintains the AR values below 3 dB in a wide frequency range, which implies that the antenna is capable of preventing a significant gain reduction caused by the distorted polarization properties in a small array.

Fig. 6(a) and (b) shows the measured and simulated radiation patterns in the *zx* and *zy* planes at 1.575 GHz. In the *zx* plane, the measured half power beamwidth (HPBW) is 75.1°, and the maximum gain is observed at $\theta = 4.8°$ with a value of 1.7 dBic. The HPBW of the pattern in the *zy*-plane is 68.7°, and a maximum value of 1.6 dBic is located at $\theta = -4.6°$. Fig. 7(a) and (b) presents the radiation patterns at 1.227 GHz, and the measured patterns show slightly broader HPBWs of 102.8° and 109.8° in the *zx* and *zy* planes, respectively. The maximum gain values of 4.8 and 4.7 dBic are observed at $\theta = 4.8°$ and $\theta = 0°$, which demonstrates that the proposed feeding structure does not exhibit serious pattern distortions in the upper hemisphere.

IV. Analysis

Fig. 8 shows the magnetic field distributions observed at 121 $\times$ 81 points in the cross section at $x = -3$ mm (-20 mm $\leq y \leq$ 20 mm, 0 mm $\leq z \leq$ 30 mm). Strong magnetic fields are confined between the lower loop and the ground with a maximum field strength of 46.6 A/m at 1.227 GHz, which implies that the lower loop operates

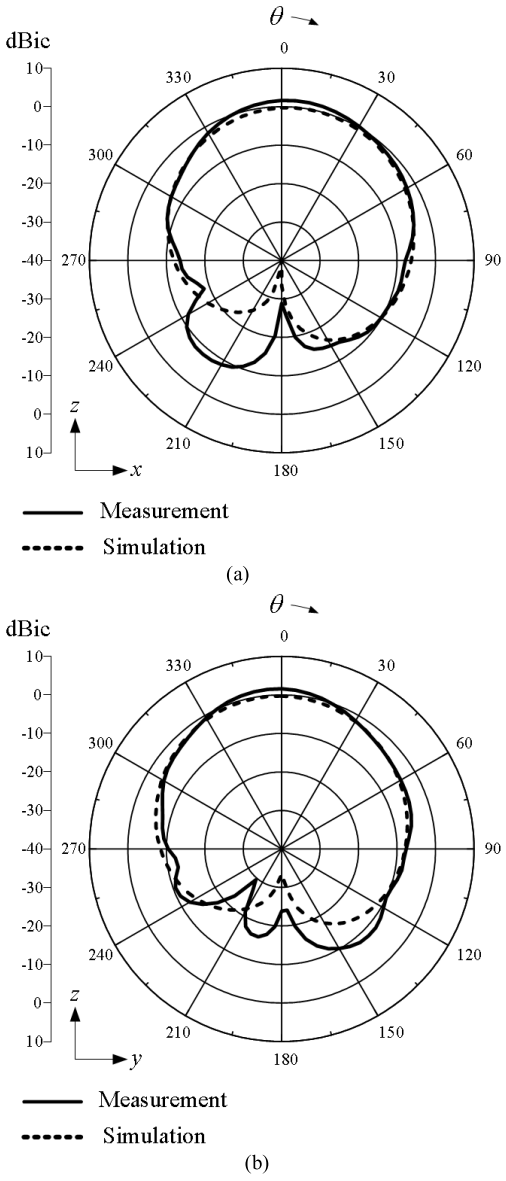

Fig. 6. 2-D patterns of the proposed antenna at 1.575 GHz. (a) *zx* plane. (b) *zy* plane.

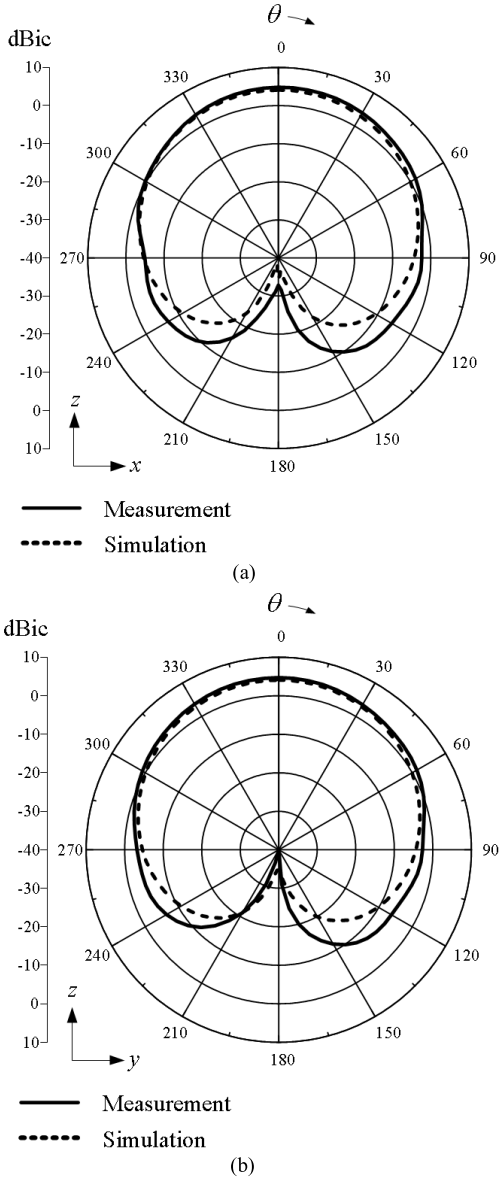

Fig. 7. 2-D patterns of the proposed antenna at 1.227 GHz. (a) *zx* plane. (b) *zy* plane.

as the dominant radiating element in the GPS L2 band. At 1.575 GHz, the upper loop is excited by the EM fields generated by the lower loop, and the two loops are tightly linked through the high-dielectric substrate with a maximum strength of 52.1 A/m.

To analyze the operating principles of the antenna from a circuit standpoint, an equivalent circuit model is developed using a data fitting method, as shown in Fig. 9(a). The circuit describes the input impedance at output port 1, while terminating the other port, denoted by output port 2, with 50-Ω impedance due to the symmetricity of the structure. The lower loop is expressed by a parallel circuit of R_{L2}, L_{L2}, and C_{L2}, and the circuit is connected to the inductance L_F representing the via pin at output port 1. Another parallel circuit, composed of R_P, L_P, and C_P, is inserted to describe a parasitic resonance at a higher frequency point above 2 GHz. The lumped elements of the upper loop are specified as R_{L1}, L_{L1}, and C_{L1} and coupled to the circuits of the lower loop through the series coupling capacitance C_C and the inductive coupling coefficient k. The values of C_C and k can be adjusted by the substrate thickness h_2 and the widths w_1 and w_2. Detailed values of the lumped elements are listed in Table II, and the input impedance of the equivalent circuit is compared to that of the EM simulation in Fig. 9(b). The results demonstrate that the operating principle of the proposed electromagnetically coupled feed is well described by the series coupling capacitance C_C and the inductive coupling coefficient k. Note that a larger value of the loop width decreases the ratio of the electric and magnetic couplings, expressed as k/C_c in Table II, since the electric coupling becomes stronger due to the increased capacitance between the upper and lower loops. In contrast, the strength of the magnetic coupling becomes relatively stronger than that of the electric coupling, when the vertical distance between the loops gets larger.

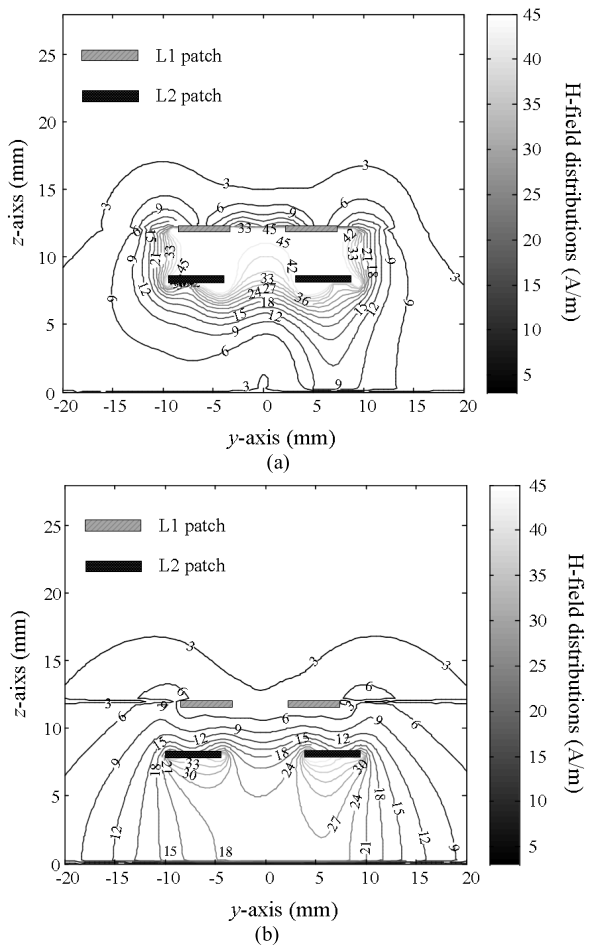

Fig. 8. H-field distribution at a cross section in the *zy* plane. (a) 1.575 GHz. (b) 1.227 GHz.

TABLE II
VALUES OF THE LUMPED ELEMENTS

Parameter	Value
L_F	6.2 nH
R_{L1}	500 Ω
L_{L1}	1.7 nH
C_{L1}	6.5 pF
R_{L2}	300 Ω
L_{L2}	1.5 nH
C_{L2}	11 pF
R_P	400 Ω
L_P	1.3 nH
C_P	5.6 pF
C_c	0.2 pF
k	0.2
k/C_c	1 pF^{-1}

Fig. 10(a) presents a comparison of reactance variations in accordance with the ratios of the electric and magnetic coupling strengths. The dashed line is calculated from the equivalent circuit in Fig. 9(a) after removing the coupling capacitance C_C, and only the inductive coupling coefficient k is varied to match the resonant frequency. The dotted line

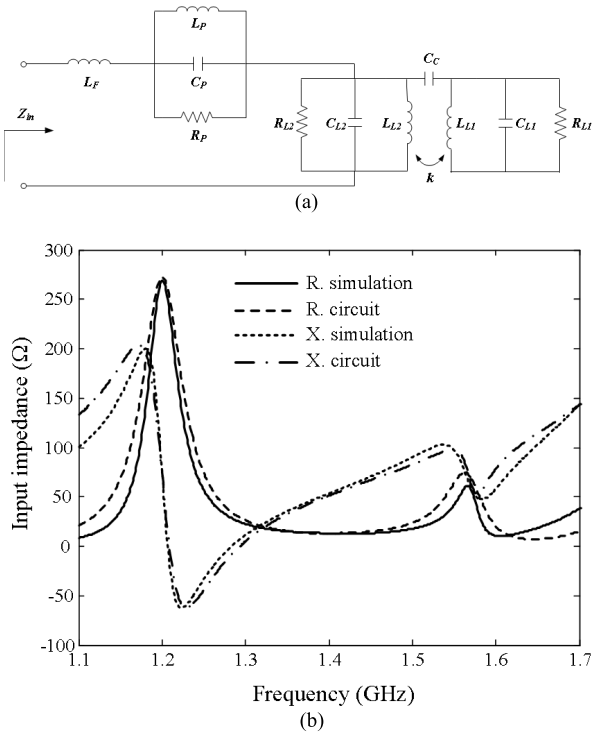

Fig. 9. Equivalent circuit model and its input impedance. (a) Circuit model. (b) Input impedance.

indicates the response when the value of k becomes zero, and the value of C_C is adjusted to maintain the same resonant point. Then, the FSR is defined to use as a figure of merit to evaluate the sensitiveness of the reactance curves, which is defined as follows:

$$\text{FSR} = \lim_{\Delta f \to 0} \left| \frac{\Delta X}{\Delta f} \right| = \lim_{\Delta f \to 0} \left| \frac{X\left(f + \frac{\Delta f}{2}\right) - X\left(f - \frac{\Delta f}{2}\right)}{\Delta f} \right| \tag{2}$$

where Δf is the frequency interval, and ΔX is the reactance variation with respect to Δf. The FSR indicates the slope of the reactance curve at each frequency point, and a small FSR implies that a low-frequency shift may occur even in the presence of the strong mutual coupling effect. The proposed feeding mechanism shows a relatively small FSR with an average value of 1 Ω/MHz; however, the maximum FSRs of the dashed and dotted lines are significantly increased from 2.2 to 3.9 Ω/MHz and 10 Ω/MHz, respectively, as shown in Fig. 10(b). This FSR increase is more significant for the standard linearly polarized loop antenna, for example, the maximum FSR is raised to 31.5 Ω/MHz near its resonant frequency of 1.575 GHz. Note that the loop antenna used in this comparison is fed by a coaxial probe, and the microstrip loop having a width of 2.3 mm and a total length of 56 mm is printed on the same ceramic substrate with a thickness of 10 mm. Thus, the ratio of the electric and magnetic coupling strengths should be carefully considered as an important design parameter to maintain frequency-insensitive reactance variations.

Fig. 11(a) and (b) shows variations in the simulated bore-sight gain of the stand-alone antenna according to different

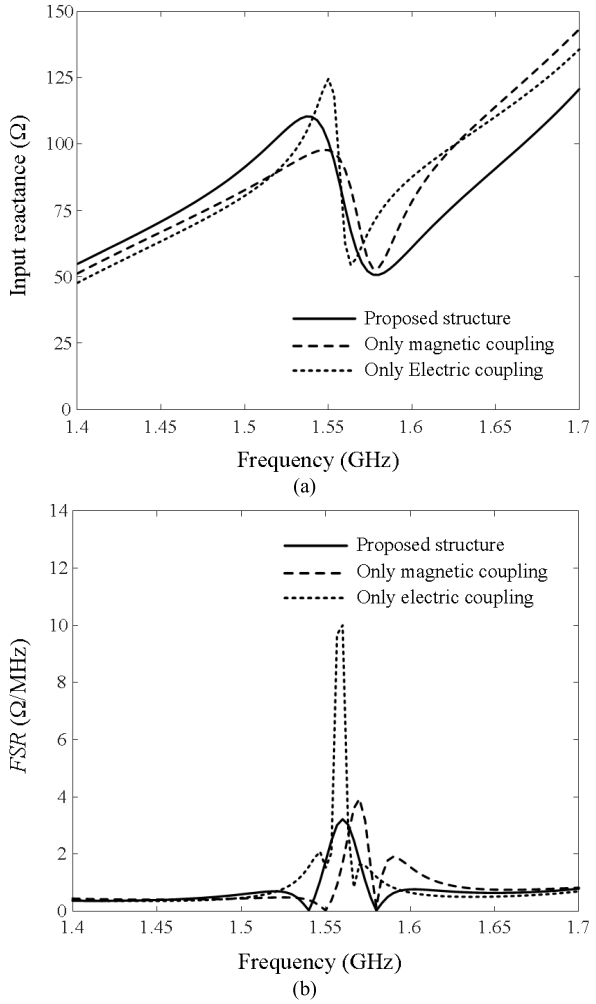

Fig. 10. Reactance and FSRs according to the feeding mechanism. (a) Reactance variations. (b) FSRs.

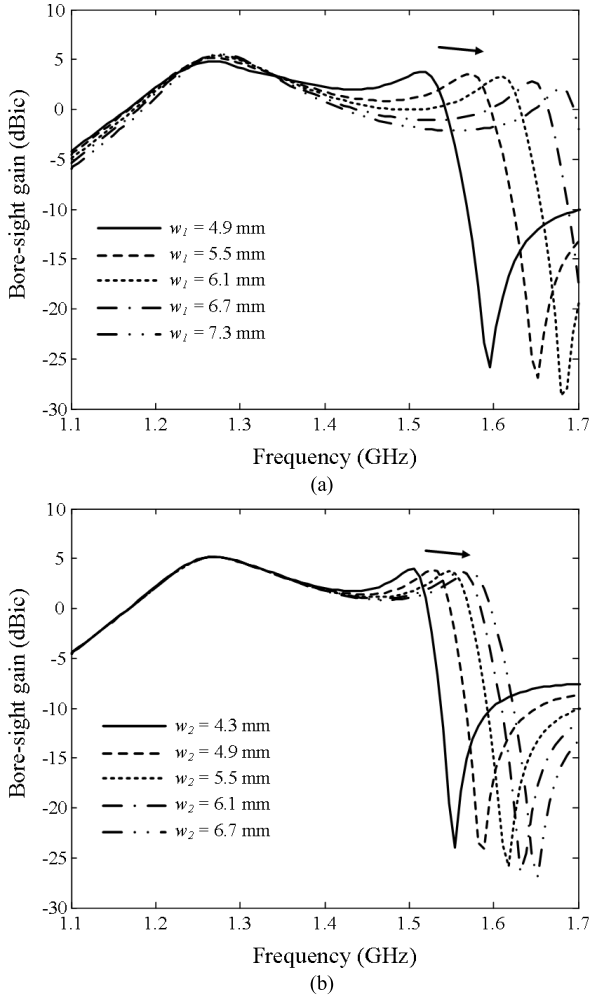

Fig. 11. Variations of bore-sight gains in accordance with the design parameters. (a) Bore-sight gains according to w_1. (b) Bore-sight gains according to w_2.

values of w_1 and w_2. The value of w_1 is increased from 4.9 to 7.3 mm at an interval of 0.6 mm, and w_2 is changed from 4.3 to 6.7 mm at an interval of 0.4 mm. The resonance of the lower loop is not affected by the strip widths because the total length of the loop is maintained as approximately one effective wavelength. By contrast, the resonant frequency of the upper loop moves toward the higher frequency band, since the strength of the electric coupling is changed by the values of w_1 and w_2.

Fig. 12 shows a comparison of the FSR according to the connection points of via pins. The proposed antenna, represented by the solid line, maintains a low FSR from 1.1 to 1.6 GHz with a mean value of 1.2 Ω/MHz. The average FSR is drastically increased to 8.0 Ω/MHz with a peak value of 185.5 Ω/MHz at 1.34 GHz, when two via pins are connected to the upper loop. Thus, the connection points of the via pins are also an important design parameter to lower the FSR to prevent significant reactance variations.

To verify the advantage of the frequency-insensitive reactance variations, we extended our research to a seven-element circular array, as shown in Fig. 13. The array consists of seven identical antennas, and each antenna is designed to have the optimized parameters listed in Table I. The microstrip loops

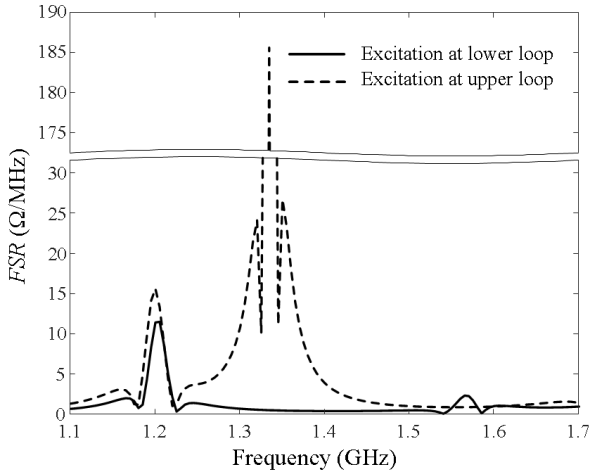

Fig. 12. FSRs according to feeding layers.

are printed on a circular ceramic substrate with a diameter of 127 mm, and the interelement spacing between antennas is 39.9 mm (0.16λ at 1.227 GHz). Fig. 14 shows a comparison of the measured and simulated bore-sight gains, when only Ant. 1 is excited while the ports of other antennas are terminated by 50-Ω loads. The measured bore-sight gains are −2.5 dBic at

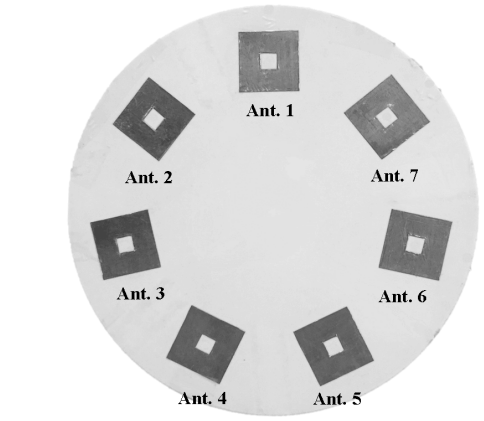

(a)

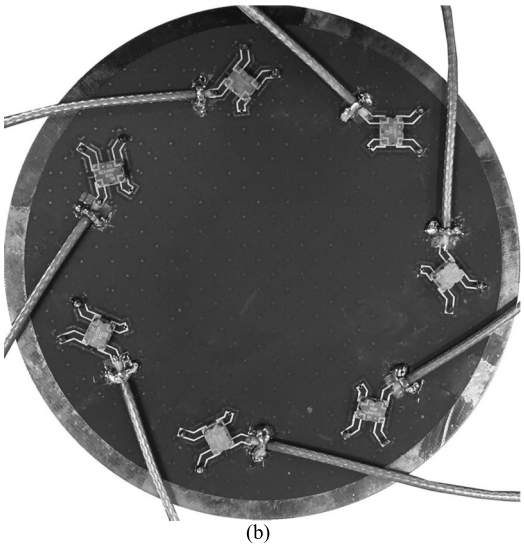

(b)

Fig. 13. Photograph of the fabricated array. (a) Top view. (b) Bottom view.

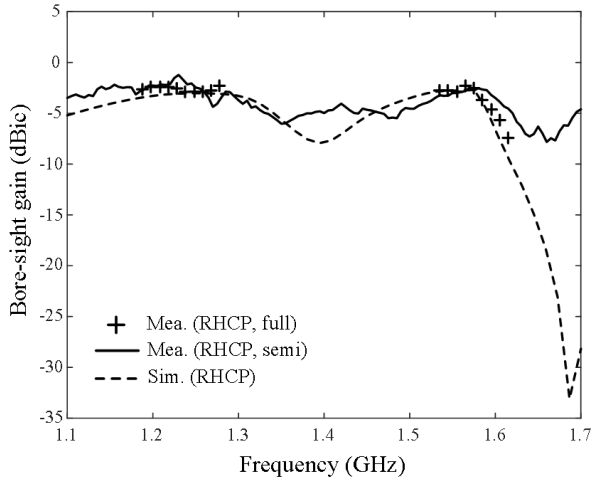

Fig. 14. Bore-sight gain for an active element pattern of Ant. 1.

both 1.575 and 1.227 GHz, and the minimum gain between two resonant frequency bands is observed at 1.353 GHz with a value of −5.8 dBic. The maximum gain deviation within the frequency range from 1.2 to 1.6 GHz is 4.8 dB

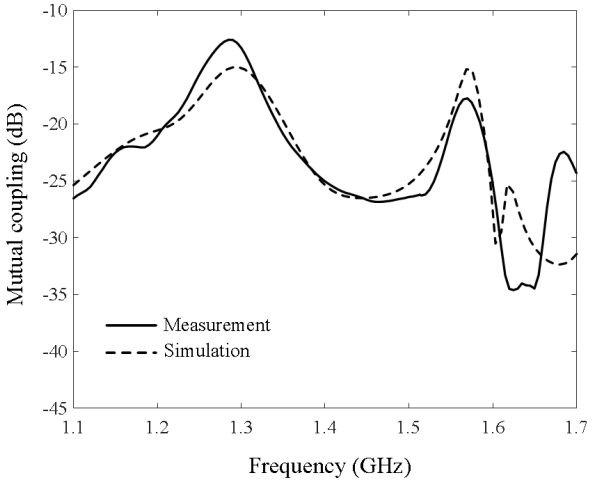

Fig. 15. Simulated and measured mutual coupling between Ant.1 and Ant. 2 of the seven-element array.

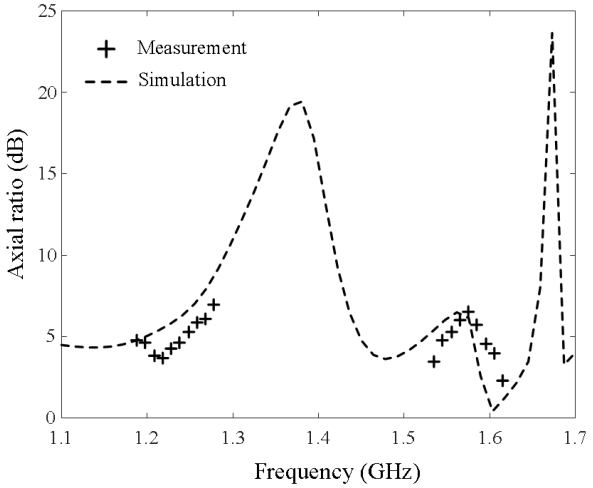

Fig. 16. Simulated and measured AR values of the seven-element array.

(maximum of −1.2 dBic at 1.23 GHz, minimum of −6 dBic at 1.35 GHz), which is drastically reduced by more than 20 dB compared to the seven-element array with conventional rectangular patch antennas whose operating principles are well known, as in [27]. The results demonstrate that the frequency-insensitive behavior of the proposed feed prevents a significant gain reduction between two resonant frequency bands, which is suitable for an extremely small array.

Fig. 15 presents the measured and simulated mutual coupling between Ant. 1 and Ant. 2 of the seven-element circular array. The measured results are specified by a solid line, and the coupling strengths at 1.575 and 1.227 GHz are −18.1 and −15.2 dB. The simulated data indicated by a dashed line show a similar trend with the measurement, and their values are −18.4 and −19.5 dB at 1.575 and 1.227 GHz, respectively. These values are relatively low compared to those for the conventional patch antenna array presented in the previous paragraph; for instance, the mutual coupling strength at 1.227 GHz is reduced by 2.7 dB due to the use of loop resonators accompanied by the proposed feeding mechanism.

Fig. 16 compares the measured and simulated ARs at Ant. 1 of the seven-element array. The measured data are presented

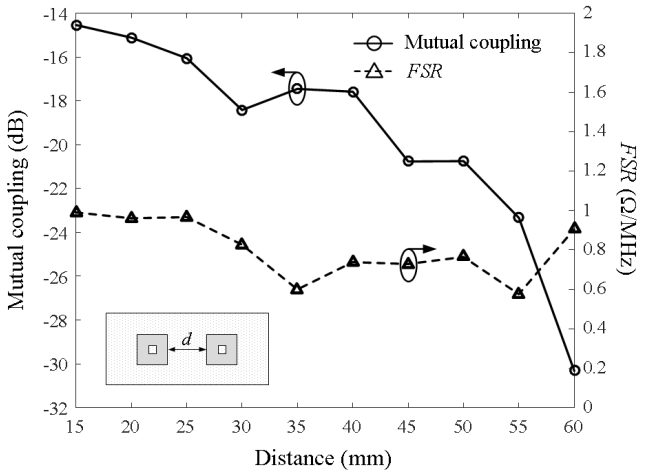

Fig. 17. Variations of the mutual coupling and the *FSR*s according to the interelement spacing d.

by "+" markers and the simulated values are specified by the dashed line. Due to the existence of the mutual coupling between antennas, the AR values at 1.575 and 1.227 GHz are raised to 6.5 and 4.2 dB for the measurement and 6.1 and 5.8 dB for the simulation, respectively.

To further verify the relation between the FSR and the mutual coupling, we calculate variations of the mutual coupling and the FSRs between two identical antennas according to the interelement spacing d from 15 mm (0.06λ) to 60 mm (0.25λ), as presented in Fig. 17. At each spacing, the FSRs and the coupling strengths are averaged using simulated values obtained at 1.227 and 1.575 GHz. As expected, the mutual coupling tends to increase from -30.3 to -14.5 dB as the interelement spacing decreases; however, the average FSRs are maintained to be less than 1 Ω/MHz in the entire range of d. This implies that the proposed antenna is capable of maintaining its frequency-insensitive behavior regardless of strong mutual coupling.

V. Conclusion

The design for a microstrip loop antenna with an electromagnetically coupled feed was proposed to achieve frequency-insensitive reactance variations. The strengths of the electric and magnetic couplings were adjusted to lower the FSR by varying the widths and the vertical placement of the microstrip loops. The feasibility of the proposed feeding mechanism was verified by measuring antenna characteristics, and the operating principle was interpreted by modeling the equivalent circuit. The stand-alone antenna had bore-sight gains of 1.5 and 4.7 dBic at 1.575 and 1.227 GHz, respectively, and the gain deviation between 1.2 and 1.6 GHz was drastically reduced to 4.8 dB for the extremely small seven-element array. The results demonstrate that the proposed antenna is suitable for maintaining an FSR of less than 3.2 Ω/MHz in the presence of strong mutual coupling.

References

[1] S. Chen, G. C. Liu, X. Y. Chen, T. Lin, X. Liu, and Z. Duan, "Compact dual-band GPS microstrip antenna using multilayer LTCC substrate," *IEEE Antennas Wireless Propag. Lett.*, vol. 9, pp. 421–423, May 2010.

[2] J.-H. Lu and K.-L. Wong, "Slot-loaded, meandered rectangular microstrip antenna with compact dual frequency operation," *Electron. Lett.*, vol. 34, no. 11, pp. 1048–1050, May 1998.

[3] Y. Sung, "Size reduction technique for slot antenna," *Electron. Lett.*, vol. 49, no. 23, pp. 1425–1426, Nov. 2013.

[4] R. Li and S. Xiao, "Compact slotted semi-circular antenna for implantable medical devices," *Electron. Lett.*, vol. 50, no. 23, pp. 1675–1677, 2014.

[5] M. He, X. Ye, P. Zhou, G. Zhao, C. Zhang, and H. Sun, "A small-size dual-feed broadband circularly polarized U-slot patch antenna," *IEEE Antennas Wireless Propag. Lett.*, vol. 14, pp. 898–901, Jun. 2015.

[6] R. Azaro, G. Boato, M. Donelli, G. Franceschini, A. Martini, and A. Massa, "Design of miniaturised ISM-band fractal antenna," *Electron. Lett.*, vol. 41, no. 14, pp. 785–786, Jul. 2005.

[7] H. Oraizi and S. Hedayati, "Miniaturization of microstrip antennas by the novel application of the giuseppe Peano fractal geometries," *IEEE Trans. Antennas Propag.*, vol. 60, no. 8, pp. 3559–3567, Aug. 2012.

[8] D. Oloumi, S. Ebadi, A. Kordzadeh, A. Semnani, P. Mousavi, and X. Gong, "Miniaturized reflectarray unit cell using fractal-shaped patch-slot configuration," *IEEE Antennas Wireless Propag. Lett.*, vol. 11, pp. 10–13, Dec. 2011.

[9] J. P. Gianvittori and Y. Rahmat-Samii, "Fractal antennas: A novel antenna miniaturization technique, and applications," *IEEE Antennas Propag. Mag.*, vol. 44, no. 1, pp. 20–36, Feb. 2002.

[10] W. Son, W. Lim, M. Lee, S. Min, and J. Yu, "Design of compact quadruple inverted-F antenna with circular polarization for GPS receiver," *IEEE Trans. Antennas Propag.*, vol. 58, no. 5, pp. 1503–1510, May 2010.

[11] S. Gupta and G. Mumcu, "Dual-band miniature coupled double loop GPS antenna loaded with lumped capacitors and inductive pins," *IEEE Trans. Antennas Propag.*, vol. 61, no. 6, pp. 2904–2910, Jun. 2013.

[12] B. Ghosh, S. K. M. Haque, and N. R. Yenduri, "Miniaturization of slot antennas using wire loading," *IEEE Antennas Wireless Propag. Lett.*, vol. 12, no. 5, pp. 488–491, Apr. 2013.

[13] G. Byun, S. Kim, and H. Choo, "Design of a dual-band GPS antenna using a coupled feeding structure for high isolation in a small array," *Microw. Opt. Technol. Lett.*, vol. 56, no. 2, pp. 359–361, Feb. 2014.

[14] D. Li, P. Guo, Q. Dai, and Y. Fu, "Broadband capacitively coupled stacked patch antenna for GNSS applications," *IEEE Antennas Wireless Propag. Lett.*, vol. 11, pp. 701–704, Jun. 2012.

[15] J. Chen, K.-F. Tong, A. Al-Armaghany, and J. Wang, "A dual-band dual-polarization slot patch antenna for GPS and Wi-Fi applications," *IEEE Antennas Wireless Propag. Lett.*, vol. 15, pp. 406–409, Jun. 2016.

[16] R. W. Ziolkowski and A. Erentok, "Metamaterial-based efficient electrically small antennas," *IEEE Trans. Antennas Propag.*, vol. 54, no. 7, pp. 2113–2130, Jul. 2006.

[17] P. Jin and R. W. Ziolkowski, "Multi-frequency, linear and circular polarized, metamaterial-inspired, near-field resonant parasitic antennas," *IEEE Trans. Antennas Propag.*, vol. 59, no. 5, pp. 1446–1459, May 2011.

[18] J. Wu, Y. Yin, Z. Wang, and R. Lian, "Broadband circularly polarized patch antenna with parasitic strips," *IEEE Antennas Wireless Propag. Lett.*, vol. 14, pp. 559–562, Mar. 2015.

[19] J. A. Kasemodel, C. C. Chen, I. J. Gupta, and J. L. Volakis, "Miniature continuous coverage antenna array for GNSS receivers," *IEEE Antennas Wireless Propag. Lett.*, vol. 7, pp. 592–595, Apr. 2008.

[20] G. Byun, H. Choo, and S. Kim, "Design of a small arc-shaped antenna array with high isolation for applications of controlled reception pattern antennas," *IEEE Trans. Antennas Propag.*, vol. 64, no. 4, pp. 1542–1546, Apr. 2016.

[21] W. Alshrafi, U. Engel, and T. Bertuch, "Compact controlled reception pattern antenna for interference mitigation tasks of global navigation satellite system receivers," *IET Microw. Antennas Propag.*, vol. 9, no. 6, pp. 593–601, Apr. 2015.

[22] *Model XC1400P-03S, Anaren*. (2012). [Online]. Available: http://www.anaren.com

[23] Y. Rahmat-samii and E. Michielssen, *Electromagnetic Optimization by Genetic Algorithms*. Hoboken, NJ, USA: Willey, 1999.

[24] *Advanced Design System (ADS), Keysight*. (2016). [Online]. Available: http://www.keysight.com

[25] *FEKO, Altair*. (2015). [Online]. Available: http://www.altair.com

[26] C. A. Balanis, *Advanced Engineering Electromagnetics*, 1st ed. New York, NY, USA: Wiley, 1989, pp. 154–168.

[27] G. Byun, H. Choo, and S. Kim, "Array configuration optimisation of dual-band controlled reception pattern antenna arrays for anisotropic ground platforms," *IET Microw. Antennas Propag.*, vol. 8, no. 8, pp. 597–603, Aug. 2014.

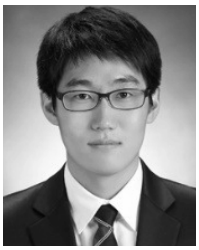

Maeng Chang Kang received the B.S. and M.S. degrees in electronic and electrical engineering from Hongik University, Seoul, South Korea, in 2015 and 2017, respectively.

He is currently a Research Engineer with the RF/Microwave Team, LIG Nex1 Co., Ltd., Yongin, South Korea. His current research interests include circularly polarized antenna design, antenna, array configuration optimization for direction finding systems, and electronically scanned active array radar.

Hosung Choo (S'00–M'04–SM'11) was born in Seoul, South Korea, in 1972. He received the B.S. degree in radio science and engineering from Hanyang University, Seoul, in 1998, and the M.S. and Ph.D. degrees in electrical and computer engineering from the University of Texas at Austin, Austin, TX, USA, in 2000 and 2003, respectively.

In 2003, he joined the School of Electronic and Electrical Engineering, Hongik University, Seoul, where he is currently a Professor. His current research interests include the use of the optimization algorithm in developing antennas and microwave absorbers, the design of small antennas for wireless communications, reader and tag antennas for RFID, and on-glass and conformal antennas for vehicles and aircraft.

Gangil Byun (S'12–M'15) received the B.S. and M.S. degrees in electronic and electrical engineering from Hongik University, Seoul, South Korea, in 2010 and 2012, respectively, and the Ph.D. degree in electronics and computer engineering from Hanyang University, Seoul, in 2015.

He is currently a Research Professor with the Research Institute of Science and Technology, Hongik University. His current research interests include circularly polarized antenna design, vehicular and aeronautic antenna design, global positioning system antenna design, antenna and array configuration optimization, and array antenna design for various adaptive beamforming applications such as direction of arrival estimation, interference mitigation, and radar.